Soft Matter

PAPER

Cite this: *Soft Matter*, 2018, **14**, 5800

Kinetic evolution of DOPC lipid bilayers exposed to α-cyclodextrins†

Monika Kluzek, * Marc Schmutz, Carlos M. Marques and Fabrice Thalmann *

Received 17th May 2018,
Accepted 15th June 2018

DOI: 10.1039/c8sm01013g

rsc.li/soft-matter-journal

Cyclodextrins are cyclic oligosaccharides capable of forming inclusion complexes with a variety of molecules, and as such have been recognized as a pharmaceutical and biotechnological asset. Cyclodextrins are known to interact with the components of cell membranes, and this correlates with a significant degree of cytotoxicity. In this work, we report on the mechanism of degradation of a model dioleoyl-phosphatidylcholine (DOPC) bilayer exposed to a solution with increasing concentrations of α-cyclodextrins. By combining optical fluorescence microscopy and quartz-crystal microbalance experiments, we study the evolution of supported lipid bilayers (SLBs) and giant unilamellar vesicles (GUVs). The rate of lipid removal is found to display a strong nonlinear dependence on the cyclodextrin concentration. A mechanism involving lipid aggregates is proposed.

1 Introduction

Cyclodextrins (CDs) are cyclic oligosaccharides formed by bacterial degradation of starch, and typically contain six (α-CD), seven (β-CD), or eight (γ-CD) glucose units linked by (1 → 4) glycosidic bonds.[1] CDs feature a relatively hydrophobic cavity which offers a suitable environment for a vast number of lipophilic molecules of different sizes (see Fig. S1, ESI†). Therefore, CDs have attracted wide interest as potential agents for drug delivery[2–4] and cholesterol sequestration,[5,6] among other applications.[3,7]

Several studies were undertaken to shed light on the possibility for cyclodextrins to extract cell membrane components, with presumably formation of molecular complexes. In particular, their action on biological membranes has been linked to hemolytic and cytotoxic effects.[8–10] Some studies attributed this hemolytic activity to the segregation and depletion of cholesterol by β-CDs. It is commonly accepted that the extraction process depends primarily on the inner diameter of the cyclodextrin cavity. Whilst the β-CD cavity composed of 7 glucose units can easily complex a cholesterol molecule, the smaller α-CD cavity size can accommodate the fatty acyl chains of lipids.[11–13]

If the cholesterol extraction activity has been studied in detail in both model membrane systems[8,14–19] and living cells,[20,21] only few studies attempted to characterize the ability of CDs to uptake lipids from cell membranes. In 2000, Nishijo *et al.*[22] demonstrated that the CD–lipid interactions are strongly dependent on the lipid chain length, the CD cavity and the nature of the external CD side groups. The importance of different parameters, such as the size of the liposomes and the lipid composition, was also studied by Hatazi *et al.*[23] Their results showed that the curvature and rigidity of the lipid membrane had a significant influence on the CD–lipid interactions. The injurious effect of CDs on lipid membranes was further explored by Giocondi *et al.*,[24] who visualized the formation of microdomains in dioleoyl-phosphatidylcholine (DOPC)/sphingomyelin (SM) lipid bilayers upon incubation with methyl-β-CD. Several authors have attributed the membrane disruptive properties of CDs to the formation of CD–lipid complexes of well defined stoichiometry. Anderson *et al.*[25] proposed the formation of CD–lipid complexes in which 4 methyl-β-CD molecules are threaded around the POPC lipid chains. Moreover, it was suggested that γ-CDs could form complexes with both phospholipid acyl chains sharing the same cavity, due to the wider secondary rim, as for instance in the case of the pyrene derivative PyrPC.[26] In the present day, it is widely accepted that cyclodextrins form complexes with the hydrocarbon chains of the phospholipid molecules.

It was demonstrated by Ohvo and Slotte[6] that the amount of lipid extraction was a function of the cyclodextrin concentration. Their results are in line with the work of Szejtli *et al.*[27] who reported that CDs at low concentrations protect erythrocytes against osmotic and heat-induced hemolysis, while larger concentrations induce cell membrane damage. Moreover, Ohtani *et al.*[8] showed that at sub-hemolytic concentrations, CDs induce changes in the erythrocyte shape.

Despite such a body of experimental work, the detailed mechanism by which cyclodextrins remove lipids from membranes remains unclear. In the present study, we investigate the

Université de Strasbourg, CNRS, Institut Charles Sadron, UPR022, 23 rue du Loess, 67034 Strasbourg Cedex, France. E-mail: monika.kluzek@weizmann.ac.il, fabrice.thalmann@ics-cnrs.unistra.fr

† Electronic supplementary information (ESI) available. See DOI: 10.1039/c8sm01013g

alteration of DOPC bilayers exposed to increasing concentrations of α-cyclodextrins, by performing experiments on supported lipid bilayers (SLBs) and giant unilamellar vesicles (GUVs). Combining laser scanning confocal microscopy (LSCM) with quartz crystal microbalance measurements (QCM-D), we observe the morphological changes of these model lipid membranes and study quantitatively the kinetics of lipid extraction. Altogether, our results provide a novel macroscopic description of α-CD mediated membrane degradation.

2 Experimental

Materials

A chloroform solution of DOPC (1,2-dioleoyl-*sn-glycero*-3-phosphocholine, $C_{44}H_{84}NO_8P$, M_w 786.11) was purchased from Avanti Polar Lipid (Birmingham, AL). DiI Stain (1,1′-dioctadecyl-3,3,3′,3′-tetramethylindocarbocyanine perchlorate $C_{59}H_{97}ClN_2O_4$, M_w 933.88) and HPTS dye (8-hydroxypyrene-1,3,6-trisulfonic acid, trisodium salt, $C_{16}H_7Na_3O_{10}S_3$, M_w 524.37) were provided by ThermoFisher Scientific (Waltham, MA, USA). α-Cyclodextrin ($C_{36}H_{60}O_{30}$ M_w 972.84), sucrose ($C_{12}H_{22}O_{11}$ M_w 342.3), glucose ($C_6H_{12}O_6$ M_w 180.16) and phosphate buffered saline (PBS) were purchased from Sigma-Aldrich (Saint-Quentin, France). All chemicals had high purity and were used without further purification.

α-Cyclodextrin solution for fluorescent SLBs and GUVs

The appropriate amount of α-cyclodextrin powder was dissolved into glucose (90 mM) solution and vortexed at least for 30 min prior to use. For all experiments, fresh solutions of α-cyclodextrin were prepared.

Giant unilamellar vesicles (GUVs)

Giant unilamellar vesicles (GUVs) of DOPC were prepared using the polyvinyl alcohol (PVA) gel assisted formation method as described by Weinberger *et al.*[28] Briefly, 200 μL of 5% (w/w) PVA solution was spread on a glass slide and dried for 30 min at 80 °C. Once the PVA-coated substrate was prepared, 5 μL of lipid in chloroform (1 mg mL^{-1}) was spread and placed under vacuum for 30 min to evaporate the organic solvent. Using a rubber gasket as a temporary chamber, the lipid film was hydrated with a sucrose solution (100 mOsm kg^{-1}) and left incubating for 60 min. After the incubation period, the GUVs were collected and transferred into Eppendorf tubes and diluted with a glucose solution (90 mOsm kg^{-1}) containing the HPTS fluorescent dye (0.4 mM). The osmolarities of the sucrose and glucose solutions were checked with a cryoscopy osmometer Osmomat 030 (Gonotec, Berlin, Germany).

Formation of supported lipid bilayers (SLBs) for measurements by laser scanning confocal microscopy

Small unilamellar vesicles (SUVs) were prepared from DOPC lipids and DiI fluorescent probes, with a 99 : 1 ratio. A mixture of lipid and dye in chloroform was dried in a small vial under a N_2 stream, and left overnight under vacuum. Sucrose solution (100 mOsm kg^{-1}) was used to re-suspend the lipids to a final concentration of 2 mg mL^{-1}. The resulting multilamellar large vesicle (MLV) suspension was sonicated using a tip sonifier (Bioblock VibraCell 72412) at the lowest power for 12 min. The SUVs thus obtained were then filtrated on a 0.22 μm membrane to remove debris from the tip, and diluted with glucose solution (90 mOsm kg^{-1}) to reach a 1 mg mL^{-1} concentration. After the injection of SUVs on the prepared glass (see next paragraph), the vesicles adsorbed at the surface undergo rupture and fusion to form an extended planar bilayer. Each supported lipid bilayer was rinsed at least 5 times with the glucose solution. Note that glucose itself is not necessary to form SUVs or SLBs. It was introduced here to facilitate the comparison between fluorescent SLB and GUV experiments.

Glass preparation for fluorescent SLBs

Before each LSCM experiment, the glass coverslip was UV/ozone treated (Novascan Ames, USA) for 15 min and rinsed with ethanol and Milli-Q (18.2 MΩ cm). Then, a second UV/ozone treatment was applied for 15 min, making the glass surface highly hydrophilic.

Laser scanning confocal microscopy measurements (LSCM)

The visualization of the lipid GUVs, the fluorescent SLBs (DiI) and the detection of fluorophores in solution (HPTS) were performed using a laser scanning confocal microscope (LSCM) Nikon Eclipse TE2000-E equipped with a Nikon d-eclipse C1 confocal unit (Nikon, Amsterdam, Netherlands). The objective was a Nikon 60× water immersion, NA 1.2 (Nikon). Excitation of DiI in supported lipid bilayers was performed at 543 nm (HeNe laser), guided to the sample by a dichromatic mirror (Nikon). The detection of the fluorescence signal was performed using a 615 nm bandpass filter and a photomultiplier (PMT). The excitation of HPTS was performed with a laser diode at 408 nm (Nikon), and the detection was performed using a 454 nm bandpass filter and a photomultiplier.

α-Cyclodextrin solution for QCM-D

The appropriate amount of α-cyclodextrin powder was dissolved into PBS buffer (0.5 mM) and vortexed at least for 30 min prior to use. For all experiments, fresh solutions of α-cyclodextrin were prepared. Blank experiments and rinsing steps were performed with the same PBS concentration.

Quartz crystal microbalance with dissipation measurements (QCM-D)

The Q-SENSE E4 system (Biolin Scientific, Stockholm, Sweden) was used to monitor the formation of SLBs on quartz surfaces coated with silicon oxide, and to follow changes in membrane properties upon exposure to α-cyclodextrin in real time. The quartz sensor crystals were placed into the QCM-D chambers and exposed to buffer, lipid and cyclodextrin solutions.

The QCM-D technique measures the resonant frequency of the overtones of the fundamental vibration of a quartz crystal, and their dephasing associated with mechanical dissipation at the surface. The resonant frequency shift is translated into an

adsorbed mass by means of the Sauerbrey equation (see ESI† and ref. 29–31 for details).

QCM-D sensor preparation

Silica-coated sensor crystals were placed into QCM-D flow chambers and cleaned by flowing ultra pure MilliQ water, sodium hydroxide solution (0.1 M) and hydrochloric acid (0.1 M). The sensors and chambers were dried under a N_2 stream. A UV-ozone cleaner (Novascan Ames, USA) was used for 45 min to treat the sensor surfaces before each experiment.

Bilayer formation and exposure to cyclodextrins

Buffer was flowed over the crystal sensors at 0.6 mL min^{-1} for *ca.* 15 min until the frequency and dissipation responses became stable. The DOPC-SUV solution was flowed over the crystals at 0.3 mL min^{-1} to form a stable supported lipid bilayer. The bilayer was rinsed with buffer in order to remove any unattached lipids. Once the baseline was stable, a 0.6 mL solution of α-cyclodextrin was added at 0.3 mL min^{-1}. The QCM-D crystals were exposed to the cyclodextrin solution during 60–90 min, after which the bilayer was rinsed again at 0.3 mL min^{-1} with a buffer solution, until the frequency stabilized. Each experiment was repeated at least three times for each concentration of α-CD.

3 Results & discussion

α-CD induced hole formation on aqueous supported lipid bilayers

To gain insight into the mechanism of α-CD–lipid bilayer interactions, we imaged the SLBs in real time. The confocal microscope was focused on the glass surface of the measuring chamber, while DOPC SUVs marked with DiI (1 mol%) were gently injected. The vesicle rupture method, used for the formation of SLBs, results in homogeneous bilayers on glass surfaces as reported elsewhere.[32,33] In order to remove vesicles in excess, the chamber was washed at least 5 times with glucose solution, and the fluorescence intensity profile and the depth profile (*z*-slices) were collected to control the quality of the SLB. Before the injection of α-CD solution into the chamber, a blank injection of glucose solution alone on the SLB was

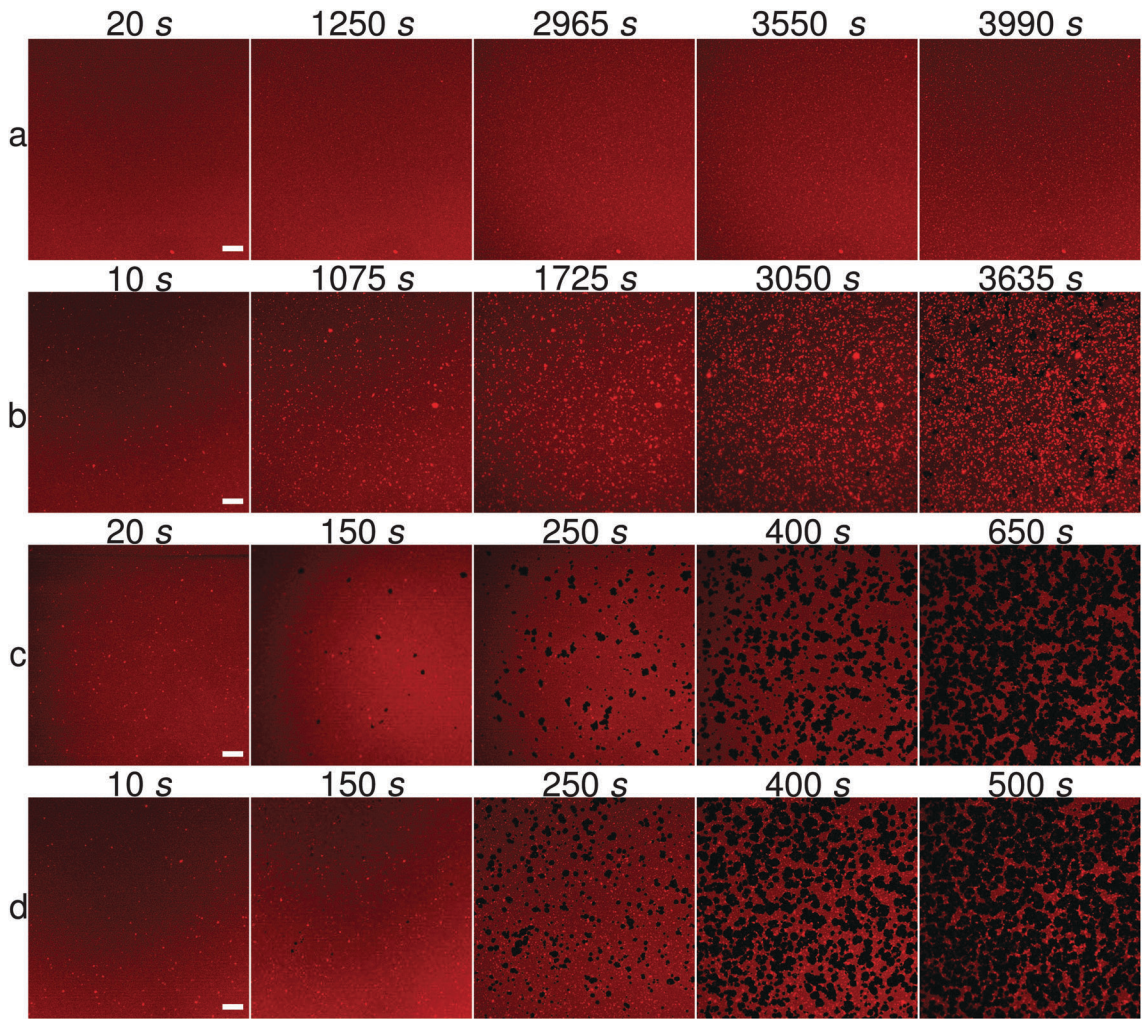

Fig. 1 Time evolution of DOPC SLB tagged with DiI at various α-CD concentrations: (a) 5 mM, (b) 10 mM, (c) 15 mM and (d) 20 mM. There is a small lag time of *ca.* 3 min between the injection of α-CD into the measuring chamber and the beginning of the microscopy acquisition. Scale bar, 10 μm.

imaged for 60 min. This step was done to ensure that the bilayer was stable, with no preexisting alterations and that the injection itself was not responsible for the formation of the defects. Fig. 1 (and Fig. S2, ESI†) shows snapshots of SLBs after the addition of α-CD at various concentrations. The LSCM imaging in the presence of a 5 mM α-CD solution revealed that the lipid membrane was only mildly affected. After 60 min acquisition, only a few small fluorescent spots were visible at the membrane surface. After the addition of the 10 mM α-CD solution, we observed the formation of many bright spots at the membrane surface. The number and the size of the spots increased continuously with the incubation time (Fig. 1b). After 60 min incubation, the first dark holes were formed. Intensity profiles showed essentially no fluorescence at the center of the holes (Fig. 2) which suggests both layers are affected by the interaction with the cyclodextrins. At higher concentrations of α-CD (15 mM and 20 mM), only 4 min incubation was needed to observe the appearance of bright spots and numerous dark holes. The size and shape evolution of the holes with time were similar for each measured concentration. Movies showing the time evolution of the fluorescent SLB are available as ESI† (Movie 1: 5 mM, Movie 2: 10 mM, Movie 3: 15 mM, Movie 4: 20 mM).

The presence of bright spots signifies that a large amount of lipids and fluorophores occupies the focal region of the scanning laser beam. Such brightness is not consistent with the darker red background associated with a single deposited bilayer. We therefore interpret the bright spots as dense lipid–cyclodextrin

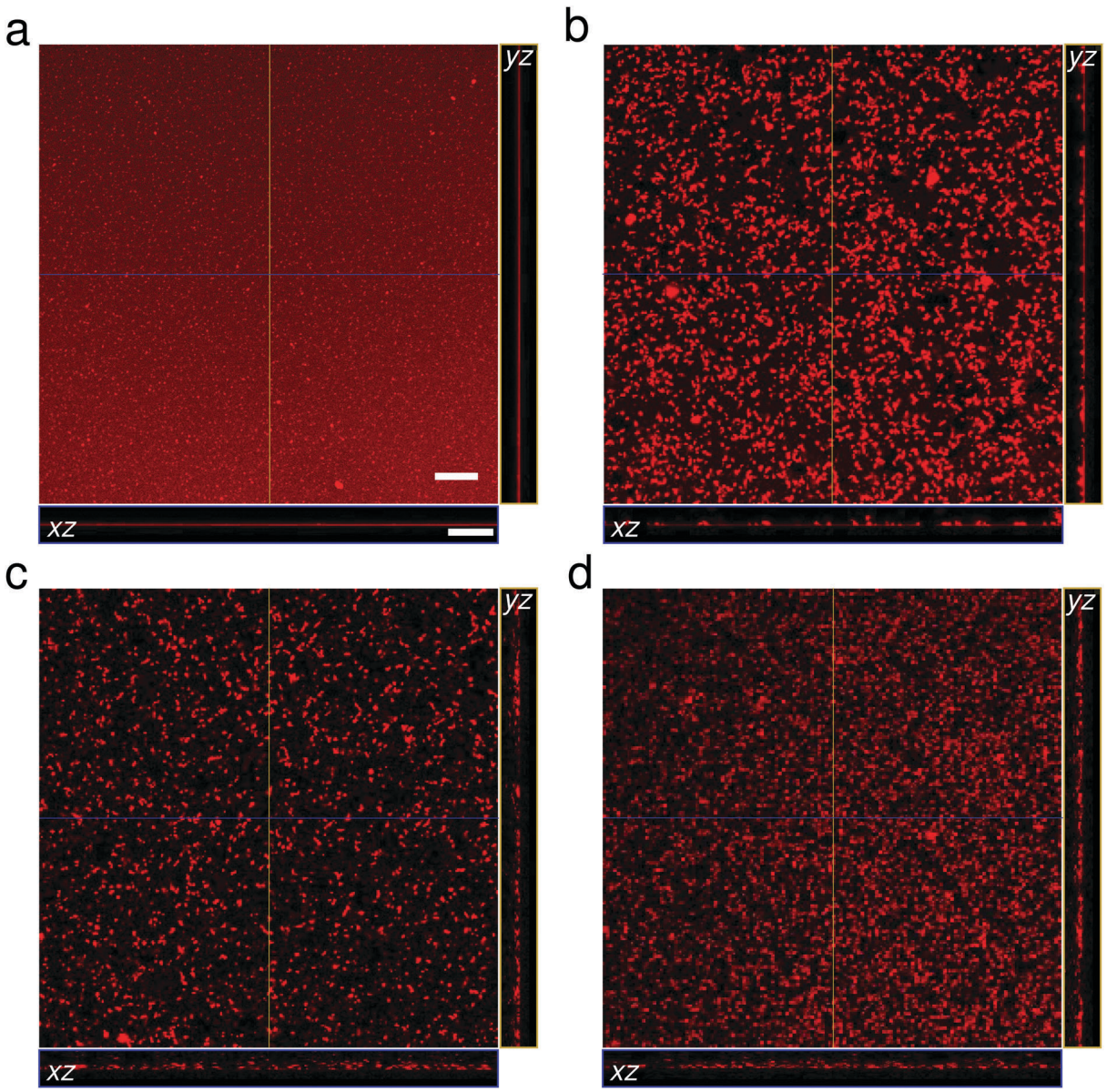

Fig. 2 Depth-resolved confocal fluorescence microscopy of DOPC SLB, 80 min after injection of α-CD concentrations of (a) 5 mM, (b) 10 mM, (c) 15 mM and (d) 20 mM. Each panel shows (*x*, *y*), (*x*, *z*) and (*y*, *z*) cuts of the original 3-dimensional image. Scale bar, 10 μm.

(and fluorophore) aggregates with a significant rearrangement of the bilayer structure. While the presence of cyclodextrin molecules within the aggregates cannot be ascertained, it seems likely that this is indeed the case, cyclodextrins being a necessary ingredient for the formation of these bright spots.

We investigated the depth profile (z-slices) of samples before and after injection of α-CD (Fig. 2). The images revealed remarkable 3-dimensional fluorescent disordered patterns above the surface. Patches of fluorescent materials could be seen floating microns above the silica surface, while still being connected to it. The size and shape of the floating patterns were variable, and no distinctive pattern characteristic of a given concentration could be found. At 10 mM CD, bright spots and floating fragments both covered densely the field of view. For the two largest concentrations, numerous floating fragments were present, with fewer bright spots visible.

The kinetic graphs, which summarize the measurements performed on the fluorescent supported lipid bilayers, are presented in Fig. 3. Using a digital image processing tool (the ImageJ plug-in),[34,35] we measured the number of holes per unit area (n_{holes}) as a function of time for each concentration. A threshold level of the fluorescent intensity was set to keep only black or white values, representing respectively the holes and the bilayer. The software then counted the number of black components. In order to avoid artefacts, we restricted ourselves to regions of area comprising between 10 and 5000 pixels, thus dismissing single pixels and larger regions formed by the merging of holes. To further avoid artefacts caused by the merging of holes, our calculations were limited to time intervals corresponding to a maximum of 15% of the total SLB area covered by holes, well before their coalescence took place.

The data are consistent with an affine increase in the number of holes per unit area with time

$$n_{\mathrm{holes}} = \gamma(t - t_0), \tag{1}$$

with t_0 a lag time, and we extracted the kinetic coefficient γ for each concentration. The rate of hole nucleation γ depends strongly on the α-CD concentration (Fig. 3a and d).

We set out to characterize the kinetics of extraction of lipids by α-CD by analyzing the area of growing single holes, and calculated the rate of lipid extraction assuming the following affine approximation

$$w_{\mathrm{holes}} = \beta(t - t_{\mathrm{cr}}), \tag{2}$$

with β the rate of lipid extraction per hole, t_{cr} the time of appearance of the hole and w_{holes} the area obtained from the number of black pixels pertaining to each hole. The resulting coefficient β, very small for concentrations smaller than a threshold value $[\mathrm{CD}]_s = 7.6$ mM, shows an affine concentration dependence $\beta = \kappa([\mathrm{CD}] - [\mathrm{CD}]_s)$ for concentrations above $[\mathrm{CD}]_s$, with a slope $\kappa = 1.06 \times 10^5\ \mathrm{s}^{-1}\ \mathrm{mM}^{-1}$ (Fig. 3b, e and also Fig. S3, ESI†).

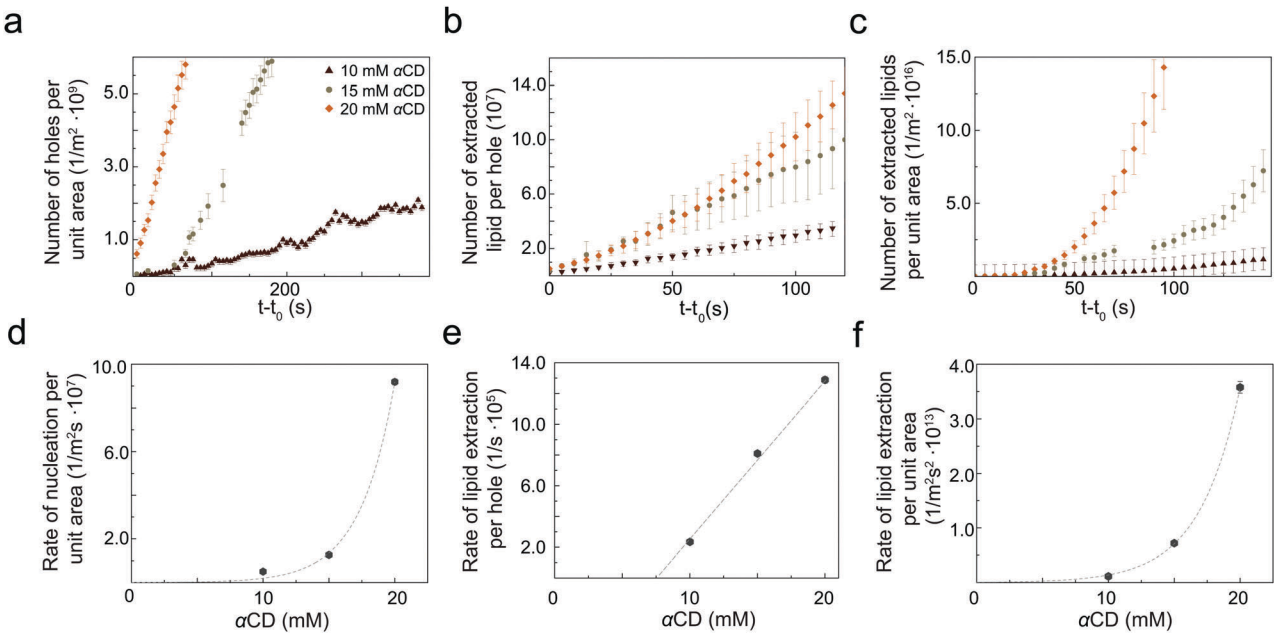

Fig. 3 (a) Number of holes per unit area *vs.* time for DOPC SLBs at 10, 15 and 20 mM α-CD concentrations. (b) Temporal evolution of the number of lipids extracted in a single hole (black area) for different α-CD concentrations. (c) Lipids extracted over time for a whole observation region of area $45 \times 10^3\ \mu\mathrm{m}^2$. (d) Dependence of the rate constant of formation of holes on the concentration (eqn (1)), corresponding to the slopes of the curves in panel a. An exponential curve (dashed line) serves as a guide to the eyes. (e) Rate β of lipid extraction per hole (eqn (2)) *vs.* concentration, corresponding to the slope of the curves in panel (b). The dashed line corresponds to a linear fit of the three data points. (f) Concentration dependence of the quadratic coefficient of eqn (4) obtained from a quadratic fit of the experimental data shown in panel (c). An exponential curve (dashed line) serves as a guide to the eyes.

According to eqn (1) and (2), the growth kinetics of the total area $\mathscr{A}_{\text{holes}}$ of the holes seen on a whole SLB image should factorize into the product of the number of holes created and the growth rate of each hole. We therefore expect that

$$\frac{\mathrm{d}\mathscr{A}_{\text{holes}}}{\mathrm{d}t} = \beta n_{\text{holes}};$$

$$\frac{\mathrm{d}n_{\text{holes}}}{\mathrm{d}t} = \gamma, \tag{3}$$

leading to

$$\mathscr{A}_{\text{holes}} = \frac{\beta\gamma}{2}(t - t_0)^2. \tag{4}$$

This quadratic model shows good agreement with experimental data (Fig. 3c and f). We report in Table 2 the average rate of lipid extraction as inferred from the growth of the dark regions in the supported lipid bilayers. This average rate $k_{\text{SLB}} = m_{15\%}/(t_{15\%}\mathscr{A}_{\text{obs}})$ is defined here as the inverse of the time $t_{15\%}$ needed to remove 15% of the initial SLB mass, multiplied by the corresponding mass removed ($m_{15\%}$) and divided by the area of the observation region ($\mathscr{A}_{\text{obs}}$).

QCM-D analysis of the resonant frequencies of SLB interacting with α-CD

The interaction between α-CD and supported DOPC bilayers was further investigated using the QCM-D technique. Monitoring overtones of the QCM-D sensor provides important information about the mechanism of action of α-CD on a lipid bilayer adsorbed on a silica (quartz) surface. Generally, changes in resonant frequencies are associated with changes in the mass of the system, either due to adsorption (a negative shift in the f value) or to desorption (a positive shift in the f value). In parallel, changes in the dissipation factor are related to changes in the mechanical properties of the membrane, whether it becomes stiffer (a decrease in D) or softer and coupled to the solvent (an increase in D).

The formation of the SLB and the consequences of its exposure to α-CDs were monitored by recording the frequency and dissipation responses of the QCM-D, as shown in Fig. 4.

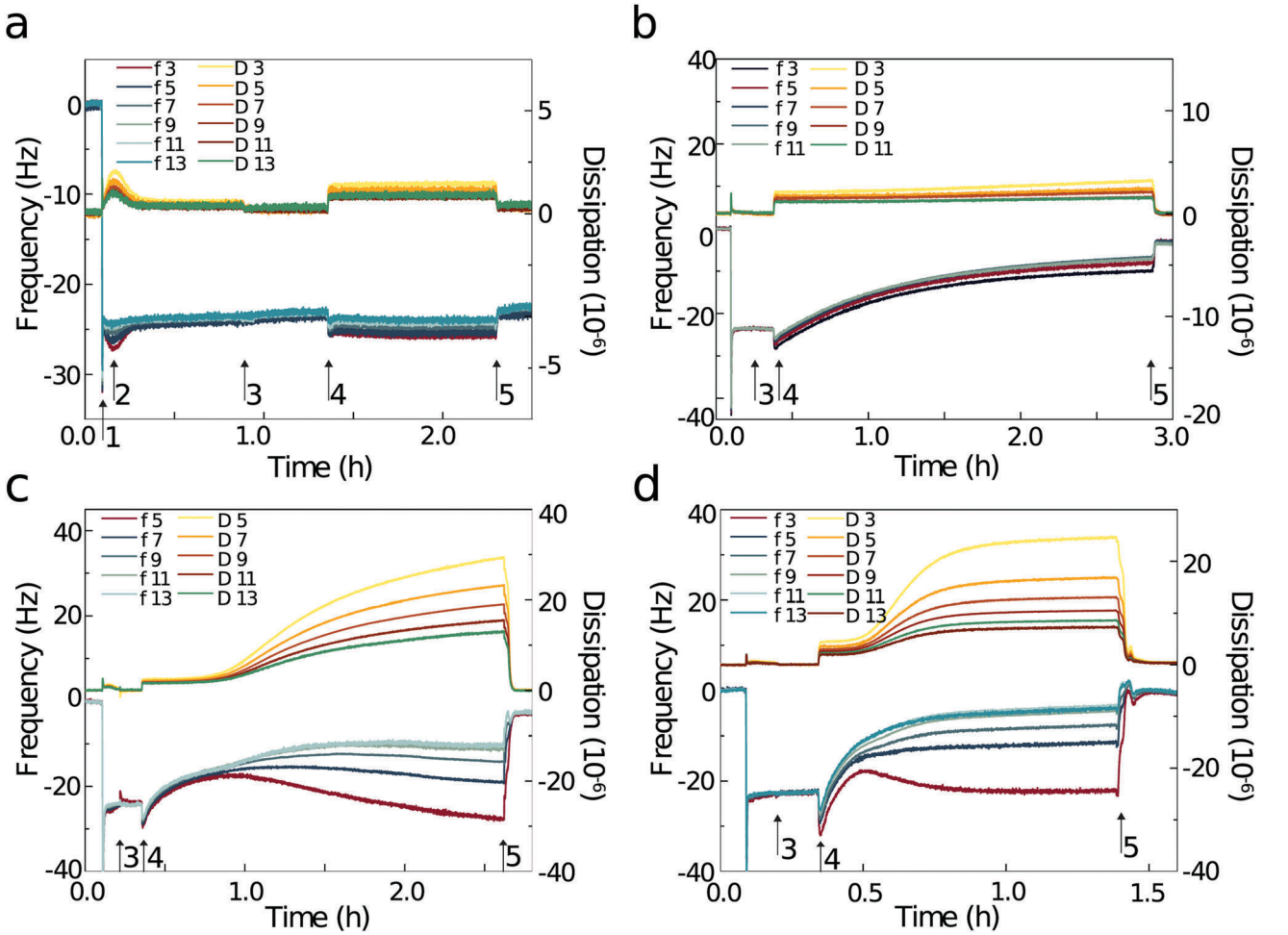

Fig. 4 Representative plots showing QCM-D frequency (f) and dissipation (D) responses of a DOPC bilayer exposed to α-CD at (a) 5 mM, (b) 10 mM, (c) 15 mM, and (d) 20 mM concentrations. Plot (a): (1) lipid vesicle injection, and (2) bilayer formation. Common to all plots: (3 and 5) buffer rinse, and (4) α-CD addition. The lines represent different overtone responses for frequency (f, lower part of the graphs, vertical axis on the left) and dissipation (D, upper part of the graphs, vertical axis on the right).

Table 1 Estimated mass changes on the QCM-D sensor, based on changes in frequencies. The mass of the deposited bilayer ($m_{bilayer}$), the mass detected at the sensor surface after the last rinse (m_{sensor}), the change in frequency after injection of α-CD ($\Delta f\alpha_{CDad}$), the corresponding mass of adsorbed α-CD ($m_{\alpha CDad}$), and the mass coverage fraction ($m_{\alpha CDad}/m_{\alpha CDmax}$). Values are shown as averages over three repeated experiments for each concentration, and the standard deviation is used as an estimate of the error

α-CD [mM]	$m_{bilayer}$ [mg] 10^{-4}	m_{sensor} [mg] 10^{-4}	$\Delta f_{\alpha CDad}$ [Hz]	$m_{\alpha CDad}$ [mg] 10^{-5}	$m_{\alpha CDad}/m_{\alpha CDmax}$
5	6.35 ± 0.32	6.29 ± 0.47	−1.74 ± 0.49	4.72 ± 1.34	0.31 ± 0.09
10	6.45 ± 0.13	0.92 ± 1.21	−2.96 ± 0.80	8.14 ± 2.18	0.53 ± 0.16
15	6.80 ± 0.22	0.88 ± 5.82	−4.56 ± 0.93	12.40 ± 2.54	0.81 ± 0.15
20	6.26 ± 0.37	0.29 ± 2.64	−5.72 ± 1.20	15.50 ± 3.25	1.01 ± 0.21

The QCM-D response upon adsorbing DOPC SUVs (in the presence of ions[36]) on silica shows a two-step process. The first step reflects the attachment of a vesicular layer to the QCM-D sensor surface, until a minimum in frequency (Δf_{min}) and a maximum in dissipation (ΔD_{max}) are reached (Fig. 4a(1)). The second step corresponds to the vesicle rupture-fusion process with the formation of a continuous SLB at the sensor surface. The membrane was then stabilized during the buffer rinse step (Fig. 4a(3)) which removed all intact vesicles and floating lipid fragments. The observed values of the frequency $\Delta f \simeq 24$ Hz and the dissipation $\Delta D \simeq 6 \times 10^{-6}$ were consistent with the formation of a stable hydrated SLB of DOPC (Table 1).[33,37,38] A buffer solution of α-CD was then added (Fig. 4a(4)) to the QCM-D chamber and was allowed to stay in contact with the bilayer for *ca.* 100 min, followed by a final buffer rinse step (Fig. 4a(5)). This final rinse allowed for comparison of the system before and after injection of α-CD.

The typical frequency response shows an initial decrease in value in all studied systems, suggesting a mass increase on the sensor surface as α-CD adsorbs on the exposed bilayer. For the lowest concentration of α-CD (5 mM), only a small decrease in Δf (<2 Hz in magnitude) was observed for each overtone, and uniform positive values of ΔD ($\simeq 1.5 \times 10^{-6}$) were recorded. However, both parameters recovered their initial values after the final buffer rinse (Fig. 4a(4)), which indicates a reversible adsorption of α-CDs on the lipid bilayer, with minor changes in the mass and viscoelasticity of the membrane. By contrast, upon addition of more concentrated α-CD solutions (15 mM and 20 mM, Fig. 4c and d), we first observed a deposition of the α-CDs at the SLB surface, followed by sharp positive shifts in frequency and dissipation with splitting of the overtones. The combined values of Δf and ΔD indicate a rapid loss of lipid mass with significant disruption and disorganization within the membrane. The magnitude decreases as the order of the overtones increases, suggesting that the transverse vibrations induced by the sensors were strongly damped on distances comparable to the membrane thickness, and that the vibration period was shorter than the bilayer internal rearrangements. The important dispersion of the dissipation parameters with frequency (overtones) is consistent with large portions of the membranes floating above the surface, dragging the outer solvent solution during their oscillatory motion, while still being connected to the surface. These results are thus compatible with an adsorption of α-CD at the surface of a membrane, followed by gradual mass removal, presumably in the form of α-CD–lipid aggregates semi-detached from the surface. Results for the 15 mM and 20 mM concentrations follow a qualitatively similar trend, indicating a similar dynamical destabilization mechanism. However, as can be seen from Fig. 4 (and Fig. S3, ESI†), it seems that the system with 20 mM α-CD reached saturation faster than the 15 mM one. Finally, exposure of DOPC-SLB to 10 mM α-CD concentration, showed an intermediate situation as compared to the 5 mM and 15 mM cases. After a short deposition of α-CDs at the membrane surface ($\Delta f = -3.0$ Hz), Fig. 4b shows positive changes in frequency for all the measured overtones. The relatively uniform increase in Δf for each overtone indicates that the lipids that remained attached to the surface oscillated homogeneously. The changes in dissipation parameter are small for all overtones, suggesting the absence of a viscoelastic mechanical response of the membrane.

The measured values of dissipation and frequency for 10, 15 and 20 mM α-CD concentrations after the final buffer rinse, show only small amounts of material remaining at the sensor surface (Table 1), which indicates that most of the lipids were removed by the α-CD molecules.

Based on the initial changes in frequency (Table 1 and Fig. 5a) and using the Sauerbrey equation (eqn (1), ESI†), we estimated the initial mass of absorbed α-CD at the membrane surface for all concentrations. Our numerical values for the initial mass were obtained from the first maximum of the frequency shift curves (10, 15 and 20 mM) and the plateau value (5 mM) in Fig. 5a.

We computed the maximal mass of α-CD that could be adsorbed onto the membrane surface, by exposing its wider rim and packing into a single hexagonal compact monolayer. Using the area of the sensor ($\mathscr{A}_{sens} = 1.54 \times 10^{-4}$ m^2) as the total area of membrane available, and taking the diameter of the wider rim equal to 13.7 Å,[39] we found an expected mass value for a dense adsorbed α-CD monolayer equal to $m_{max} = 1.54 \times 10^{-4}$ mg.

The ratio of the measured mass deposited at the quartz surface to m_{max} defines a covered fraction (Fig. 5b and Table 1). Interestingly, the experimental covered fraction increases linearly with α-CD concentration, reaching a maximum value close to 1 at 20 mM. It should be stressed that our model relies on a uniform monolayer of adsorbed α-CD, whereas more complex associations of the CDs with the membrane have been reported.[40–42]

By following changes in mass on the QCM-D sensor in the linear regime immediately following the initial adsorption (Fig. 5a) and dividing the loss of mass by the area of the sensor $\mathscr{A}_{sens}$, we calculated the rates $k_{QCM\text{-}D}$ of lipid removal by α-CD. While being defined in a totally independent way, the

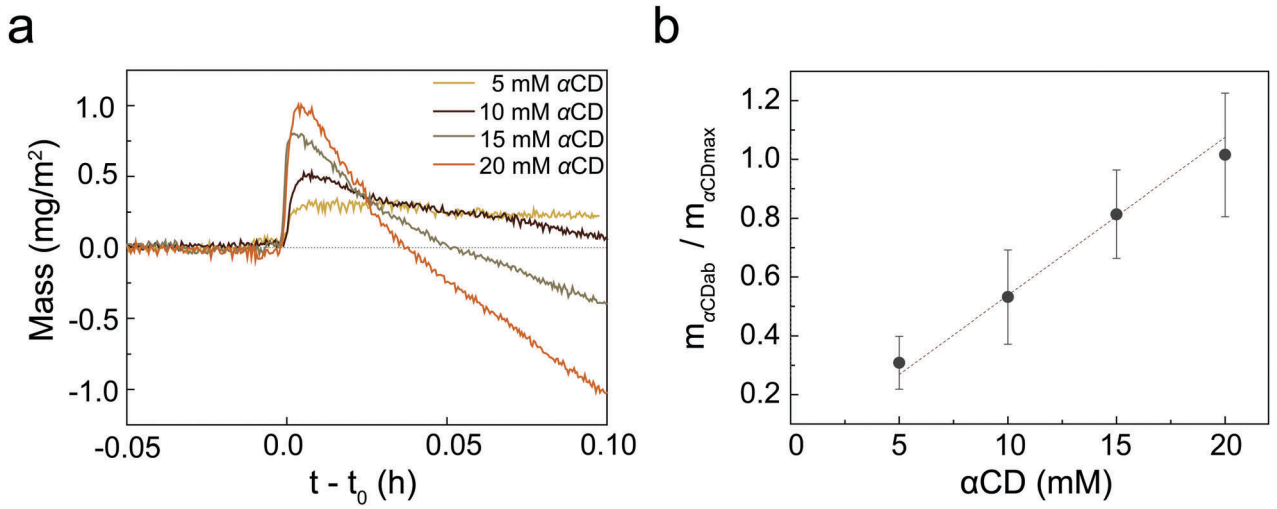

Fig. 5 (a) Changes in mass on the sensor after the injection of α-CD at various concentrations (data for the 7th overtone). (b) Cover fraction equivalent to one monolayer of α-CD on the membrane surface. The dashed line represents the best linear fit.

Table 2 Rate of lipid extraction by α-CD calculated from supported lipid bilayer (SLB) and giant unilamellar vesicle (GUV) measurements using QCM-D and LSCM techniques. Values are shown as averages of at least two measurements for each concentration, and the standard deviation is used as an estimate of the error

	SLB LSCM	SLB QCM-D	GUVs LSCM
α-CD [mM]	k_{SLB} [mg m^{-2} s^{-1} 10^{-4}]	$k_{QCM\text{-}D}$ [mg m^{-2} s^{-1} 10^{-4}]	k_{GUVs} [mg m^{-2} s^{-1} 10^{-4}]
10	2.98 ± 0.08	9.61 ± 0.02	103 ± 56
15	5.64 ± 0.23	18.40 ± 0.05	139 ± 103
20	18.70 ± 0.52	58.60 ± 0.04	399 ± 234

fluorescent SLB k_{SLB} and QCM-D $k_{QCM\text{-}D}$ rates correlate well (Table 2).

Dynamics of GUV degradation by α-CD

To gain more insight into the membrane-disruptive mechanism of α-CD, we observed isolated giant unilamellar vesicles. Fig. 6 shows the typical temporal evolution of GUVs following exposure to 10 mM α-CD. After the α-CD aqueous solution was injected into the observation chamber, defects began to develop from the GUV surface (Fig. 6, white and black arrows). The movie shows an anomalous aggregate, or protrusion, at the vesicle surface. Beside protrusions being visible at the surface, the GUV shrank gradually, while keeping its spherical shape until the final stages. At the beginning of the shrinking stage and during a short period, the vesicle decreased in size but its interior showed no fluorescence. Then, the vesicle compartment steadily increased its fluorescence intensity, indicating a loss of integrity of the membrane and exchange of larger molecules between the vesicle interior and the external solution (Fig. 6 and Movie M5, ESI†). The fact that the HPTS fluorophore used in this measurement has a sizable molecular weight (M_w = 524.37 Da) suggests that membrane permeabilization occurred though pore formation. The entire process took place within 10 min following cyclodextrin injection. This indicates that poration and membrane protrusion occurred in parallel, and are two facets of the same underlying membrane degradation mechanism. Concentrations of α-CD larger than 5 mM were required to make the degradation of GUVs effective.

The apparent diameter of a few selected vesicles was measured and represented as a function of time (Fig. 7 and Fig. S4, ESI†). Interestingly, the apparent diameter, and not the area, decreases linearly with time. This shrinking dynamics suggests that losses in the membrane surface are compensated for by corresponding losses of intravesicular water. Since vesicles remain spherical at all times but the very end, we suggest that lipid extraction from GUVs is a continuous process lasting until the reservoir of available lipids is exhausted. The persistent spherical shape suggests also that under our working conditions, osmotic imbalance is not a significant driving force for the shrinking mechanism.

As for SLB measurements, we noticed a faster than linear evolution of the lipid extraction kinetics with the concentration of α-CD in the observation cell. At a low concentration of 5 mM, vesicles remained unaltered during at least 40 min of acquisition (data not shown). Conversely, under larger α-CD concentrations, a morphological response was detected after only a few minutes of observation.

To better quantify the mechanism of the observed α-CD–lipid bilayer shrinking phenomenon, we converted the observed initial decrease in area into a loss of lipid mass per area of the vesicle, based on a commonly accepted value of the area per lipid for a DOPC bilayer (70 Å^2).[43] This resulted in an average rate of lipid extraction k_{GUVs} (Table 2). It is worth noting that the GUVs do not contain α-CDs in their interior compartment until they are mixed with the α-CD solution. During the initial stage of vesicle shrinking, the intact bilayer acts as a barrier against HPTS penetration, and presumably against α-CD penetration as well. Therefore, one can compare the GUV and the SLB situations, as in both cases the alteration results from the action of agents present only on one side of the bilayer.

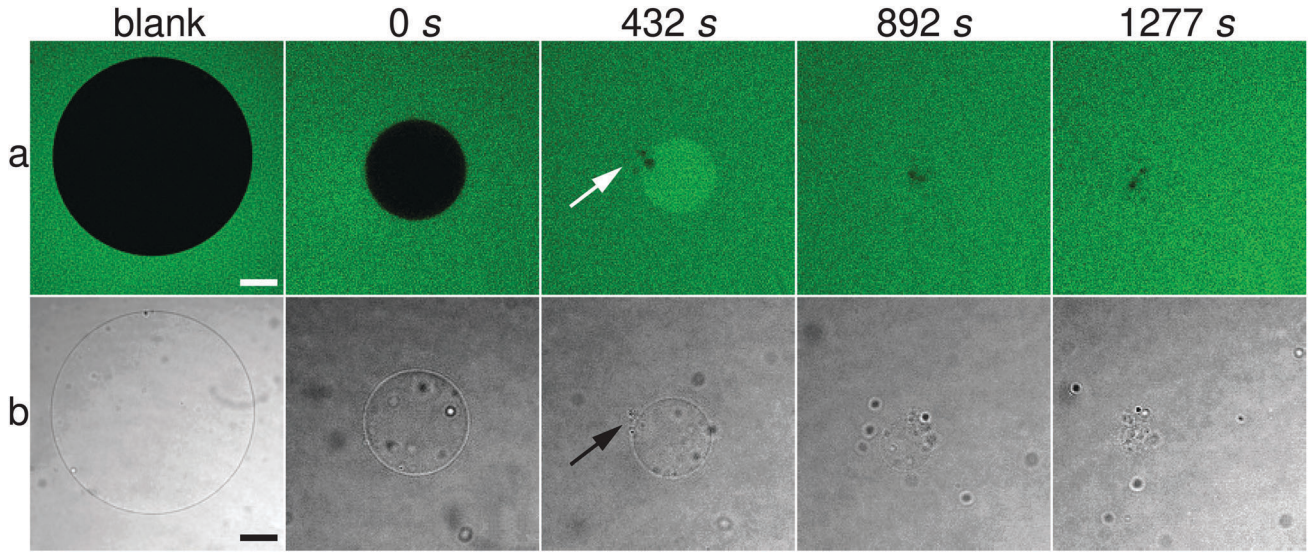

Fig. 6 Time evolution of DOPC GUVs interacting with 10 mM α-CD. (a) Laser scanning confocal microscopy of GUVs in a solution containing the water soluble dye HPTS, and (b) corresponding bright field images. Arrows show an anomalous aggregate at the vesicle surface (bright and dark spots, respectively). There is a small lag time of *ca.* 3 min between the GUV/α-CD mixing and the beginning of the microscopy acquisition. Scale bar, 10 μm.

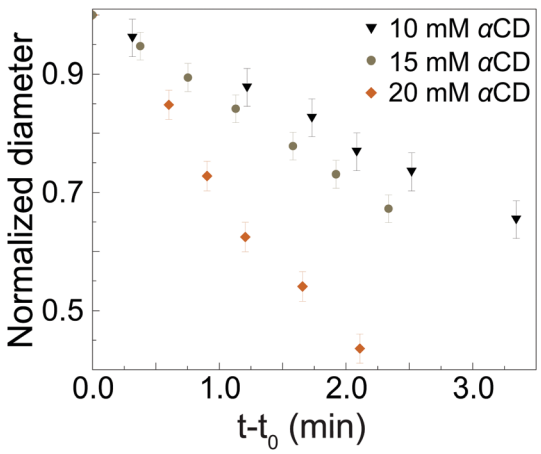

Fig. 7 Changes in GUV diameter upon interaction with α-CD at various concentrations, t_0 observation lag time.

Discussion

Both supported and vesicle lipid bilayers were found to be strongly degraded by the alpha-cyclodextrins. The nature and the kinetics of the degradation were consistently dependent on the α-CD concentration level in solution. At 5 mM α-CD, the bilayer was only marginally altered. The mass adsorption on the SLB was reversible, the SLB appearance stayed uniform for hours and GUVs did not evolve for at least 40 min. In contrast, a 15 and 20 mM concentration level of α-CD brought about fast, strong and irreversible alterations of the bilayers. The entire mass of the SLB was removed while a dissipation level typical of a poorly bound membrane was observed. The fluorescent images of the SLB showed many detached patches of membranes along with fast growing dark regions with no lipid in contact with the surface. GUV shrinking and permeabilization were fast, although vesicles retained their spherical shapes. Spots at the vesicle surface were visible. The 10 mM case differed qualitatively from the two previous limits. The bilayer evolved in a non-reversible way, but at a significantly slower rate. The degradation then seemed to be both homogeneous and progressive. Bright spots covered the fluorescent SLBs, followed by many slowly growing black holes. The QCM-D signal showed an irreversible loss of mass, but the amount of dissipation remained low with almost superimposed overtones. A slower GUV contraction was observed.

All these observations show a strongly non linear concentration dependence of the mechanism, both quantitatively and qualitatively. They bear the hallmark of a cooperative multimolecular process. It is likely that the presence of protrusions/aggregates at the GUV surface (Fig. 6) mirrors the similar protrusions/aggregates seen in SLB images (Fig. 1 and 2). Lipid removal from the bilayers of both systems is therefore due to the presence of dense CD–lipid aggregates at the surface. Based on these observations, the following mechanism naturally emerges. Aggregates mixing lipids and cyclodextrins grow at the expense of the bilayer and put it under tension. After some time, the membrane is severely altered, causing the porosity of the vesicle and the appearance of dark holes in the supported bilayer. Aggregates need not be bilayers and could very well display a different molecular organization built on tight cyclodextrin–lipid interactions. Future investigations of the nature of the aggregates by electron microscopy should further clarify this question.

Table 2 reveals that the lipid removal kinetic coefficients for SLBs and GUVs differ significantly. As the driving force acting on bilayers is assumed to be common to both systems, the difference in kinetics is likely to originate from a different dissipation mechanism opposing lipid removal. In the case of SLBs, interaction with the surface as well as lipid bilayer friction are strong. This could explain why the rates are

relatively lower. In the case of GUVs, the dominant dissipation mechanism is likely the viscous resistance of the internal solvent that is expelled during the vesicle shrinking stage. Assuming that the solvent flow across the bilayer is proportional to the vesicle area A, and that the interaction with α-CD puts the membrane under constant tension, therefore increasing the internal pressure due to Laplace's law, the time derivative of the inner volume V is expected to comply with the following equation

$$\zeta \frac{\mathrm{d}V}{\mathrm{d}t} = -A, \tag{5}$$

with constant rate ζ. This behavior leads in turn to a linear decrease in vesicle diameter, as observed.

4 Conclusion

Using a combination of confocal microscopy and quartz crystal microbalance experiments, we studied the mechanism of degradation of a DOPC bilayer exposed to increasing concentrations of α-CD in solution. For the first time, we could complement the usual QCM-D mass measurements with fluorescent imaging of SLBs under very similar conditions.

Our results favor a molecular mechanism of lipid extraction based on the formation of lipid–cyclodextrin rich aggregates that promote a local alteration of the bilayer (lipid protrusions and spots). These aggregates grow at the expense of the bilayer, either shrinking and creating defects in the vesicles, or tearing apart the supported bilayers, with the creation of dark holes.

The kinetics of the bilayer degradation is strongly dependent on the α-CD concentration. With little or slow effects at a concentration of 5 mM, the evolution is both fast and disruptive at concentrations of 15 and 20 mM. The 10 mM case is an intermediate situation with irreversible loss of mass but little apparent changes in the bilayer structure. Beyond concentration, we anticipate that other factors such as membrane cholesterol content or temperature would also influence the kinetics of degradation.

Our study confirms the potency of α-CD as a model membrane disruptive agent, which become aggressive to the lipid bilayer at concentrations larger than 10 mM. We suggest that our observations could be related to the cytotoxic character of α-cyclodextrins that is sometimes reported.

Conflicts of interest

There are no conflicts to declare.

Acknowledgements

M. Kluzek, F. Thalmann, C. M. Marques, and M. Schmutz all acknowledge funding from the European FP7-MSCA Initial Training Network (ITN) SNAL 608184 (Smart nano-objects for alteration of lipid-bilayers) to support the work. M. Kluzek thanks Olivier Félix for support with QCM-D experiments.

References

1 M. Monteil, M. Lecouvey, D. Landy, S. Ruellan and I. Mallard, *Carbohydr. Polym.*, 2017, **156**, 285–293.
2 S. S. Jambhekar and P. Breen, *Drug Discovery Today*, 2016, **210**(2), 356–362.
3 T. Loftsson and D. Duchêne, *Int. J. Pharm.*, 2007, **3290**(1–2), 1–11.
4 J. P. Litz, N. Thakkar, T. Portet and S. L. Keller, *Biophys. J.*, 2016, **1100**(3), 635–645.
5 E. M. M. Del Vallee, *Process Biochem.*, 2004, **390**(9), 1033–1046.
6 H. Ohvo and P. J. Slotte, *Biochemistry*, 1996, **350**(24), 8018–8024.
7 H. Arima, T. Higashi and K. Motoyama, *Ther. Delivery*, 2012, **30**(5), 633–644.
8 Y. Ohtani, T. Irie, K. Uekama, K. Fukunaga and J. Pitha, *Eur. J. Biochem.*, 1989, **1860**(1–2), 17–22.
9 T. Irie and K. Uekama, *J. Pharm. Sci.*, 1997, **860**(2), 147–162.
10 G. Piel, *et al.*, *Int. J. Pharm.*, 2007, **3380**(1–2), 35–427.
11 F. Fauvelle, J. C. Debouzy, S. Crouzy, M. Göschl and Y. Chapron, *J. Pharm. Sci.*, 1997, **860**(8), 935–943.
12 F. Fauvelle, J. C. Debouzy, R. Nardin and A. Gadelle, *Bioelectrochem. Bioenerg.*, 1994, **330**(1), 95–99.
13 R. Leventis and J. R. Silvius, *Biophys. J.*, 2001, **810**(4), 2257–2267.
14 E. Róka, *et al.*, *Molecules*, 2015, **200**(11), 20269–20285.
15 V. Monnaert, S. Tilloy, H. Bricout, L. Fenart, R. Cecchelli and E. Monflier, *J. Pharmacol. Exp. Ther.*, 2004, **3100**(2), 745–751.
16 D. Ondo, *J. Chem. Thermodyn.*, 2016, **97**, 235–243.
17 R. Diaz-Salmeron, I. Chaab, F. Carn, M. Djabourov and K. Bouchemal, *J. Colloid Interface Sci.*, 2016, **482**, 48–57.
18 J. P. Litz, N. Thakkar, T. Portet and S. L. Keller, *Biophys. J.*, 2016, **1100**(3), 635–645.
19 C. A. Lopez, A. H. de Vries and S. J. Marrink, *Sci. Rep.*, 2013, **3**, 2071.
20 L. Leclercq, Q. Lubart, J. M. Aubry and V. Nardello-Rataj, *Langmuir*, 2013, **290**(21), 6242–6252.
21 E. Sabadini, F. do Egidio and T. Cosgrove, *Langmuir*, 2013, **290**(15), 4664–4669.
22 J. Nishijo, *et al.*, *Chem. Pharm. Bull.*, 2000, **480**(1), 48–52.
23 P. Hatzi, S. Mourtas, P. G. Klepetsanis and S. G. Antimisiaris, *Int. J. Pharm.*, 2007, **3330**(1), 167–176.
24 M.-C. Giocondi, P.-E. Milhiet, P. Dosset and C. Le Grimellec, *Biophys. J.*, 2004, **860**(2), 861–869.
25 T. G. Anderson, A. Tan, P. Ganz and J. Seelig, *Biochemistry*, 2004, **430**(8), 2251–2261.
26 K. Tanhuanpää, K. Cheng, K. Anttonen, J. A. Virtanen and P. Somerharju, *Biophys. J.*, 2001, **810**(3), 1501–1510.
27 J. Szejtli, T. Cserháti and M. Szögyi, *Carbohydr. Polym.*, 1986, **60**(1), 35–49.
28 A. Weinberger, *et al.*, *Biophys. J.*, 2013, **1050**(1), 154–164.
29 K. F. Wang, R. Nagarajan and T. A. Camesano, *Biophys. Chem.*, 2015, **196**, 53–67.
30 F. Höök, B. Kasemo, T. Nylander, C. Fant, K. Sott and H. Elwing, *Anal. Chem.*, 2001, **730**(24), 5796–5804.
31 F. Johannsmann, *Springer Ser. Chem. Sens. Biosens.*, 2007, **50**, 49–109.

32 C. A. Keller, K. Glasmästar, V. P. Zhdanov and B. Kasemo, *Phys. Rev. Lett.*, 2000, **84**, 5443–5446.
33 J. A. Jackman, M. Kim, V. P. Zhdanov and N.-J. Cho, *Phys. Chem. Chem. Phys.*, 2015, **180**(4), 3065–3072.
34 C. A. Schneider, W. S. Rasband and K. W. Eliceiri, *Nat. Methods*, 2002, **90**(7), 671–675.
35 ImageJ. Particle Analysis, 2017, URL https://imagej.net/Particle_Analysis.
36 B. Seantier and B. Kasemo, *Langmuir*, 2009, **250**(10), 5767–5772.
37 R. P. Richter, R. Bérat and A. R. Brisson, *Langmuir*, 2006, **220**(8), 3497–3505.
38 K. F. Wang, R. Nagarajan, C. M. Mello and T. A. Camesano, *J. Phys. Chem. B*, 2011, **1150**(51), 15228–15235.
39 J. Szejtli, *Chem. Rev.*, 1998, **980**(5), 1743–1754.
40 C. A. Lopez, A. H. de Vries and S. J. Marrink, *PLoS Comput. Biol.*, 2011, **70**(3), e1002020.
41 C. A. Lopez, A. H. de Vries and S. J. Marrink, *Sci. Rep.*, 2013, **3**, 2071.
42 E. Mixcoha, J. Campos-Terán and A. Piñeiro, *J. Phys. Chem. B*, 2014, **1180**(25), 6999–7011.
43 J. F. Nagle and S. Tristram-Nagle, *Biochim. Biophys. Acta, Rev. Biomembr.*, 2000, **14690**(3), 159–195.

